ORIGINAL ARTICLE

Journal
*of the* American Ceramic Society

# Flash-sintering of magnesium aluminate spinel (MgAl$_2$O$_4$) ceramics

Hidehiro Yoshida[1,a] | Papiya Biswas[2,a] | Roy Johnson[2] | Mantravadi Krishna Mohan[3]

[1]National Institute for Materials Science, Sengen, Tsukuba, Ibaraki, Japan

[2]International Advanced Research Centre for Powder Metallurgy and New Materials, Hyderabad, India

[3]National Institute of Technology, Warangal, India

**Correspondence**
Hidehiro Yoshida, National Institute for Materials Science, Sengen, Tsukuba, Ibaraki, Japan.
Email: yoshida.hidehiro@nims.go.jp

**Abstract**

The sintering behavior of commercially available MgAl$_2$O$_4$ spinel was investigated under DC electric field in a range of 0 and 1000 V/cm. Flash-sintering results in densification close to theoretical density at 1410°C under the DC field of 1000 V/cm, in comparison to the higher sintering temperature of 1650°C in case of conventional sintering. It was observed that the fields less than 750 V/cm had no significant effect on the densification behavior. An abrupt increase in power dissipation was observed corresponding to the occurrence of the flash event. A significant enhancement in grain size was observed in case of flash-sintered dense spinel samples. The gradual increase in the specimen conductivity observed in the electric field-assisted sintering (FAST) regime led to Joule heating within the specimen. The increased specimen temperature triggered further increment of current and Joule heating, resulting in the immediate densification.

**KEYWORDS**
densification, electrical conductivity, grain growth, sinter/sintering, spinels

## 1 | INTRODUCTION

### 1.1 | Sintering of spinel

Magnesium aluminate spinel (MgAl$_2$O$_4$) is a synthetic material with excellent chemical, thermal, dielectric, and mechanical properties, and has been therefore used for wide range application in thermo-structural implementations such as a lining for steel ladle, cement rotary kiln, and glass furnace regenerator.[1-7] However, dense spinel is difficult to fabricate.[7] In earlier works, dense polycrystalline spinel has been obtained through high-temperature conventional sintering (typically >1500°C),[8,9] hot-pressing,[10-12] hot isostatic pressing (HIP),[13-16] spark plasma sintering,[17,18] and microwave sintering.[19-21] Electric field-assisted sintering (FAST) is gaining interest in recent years due to the accelerated consolidation compared to conventional, pressureless sintering.[22-26] In particular, flash-sintering,[27,28] where densification occurs almost immediately (typically <5 seconds) under high DC fields, has attracted

extensive attention as an innovative sintering technique. The flash-sintering has been demonstrated in various ceramics,[29-39] and nearly full density has been achieved at relatively low furnace temperature for very short time. This not only results in significant retardation of grain growth but also substantial economic benefits. In this study, flash-sintering was employed to consolidate MgAl$_2$O$_4$ ceramic from commercially available spinel powder. Though the various methodologies for the sintering of spinel have been investigated, flash-sintering of spinel has not been reported so far. We demonstrate that DC field at 1000 V/cm can trigger flash-sintering resulting in dense polycrystalline MgAl$_2$O$_4$ spinel ceramics.

### 1.2 | Ionic mass transport in spinel

MgAl$_2$O$_4$ exhibits mainly ionic conduction at temperatures beyond 400°C.[9] The values for electric conductivity of MgAl$_2$O$_4$ reported in the literature significantly depend on the composition, microstructure and temperature. However, it has been widely accepted that magnesium cations (Mg$^{2+}$) or vacancies ($V''_{Mg}$ in Kröger-Vink notation) are the

---

[a]Member, The American Ceramic Society.

main charge carriers and the conductivity values are not greatly influenced by oxygen partial pressure.[40-44] In contrast, the rate-controlling mechanism for sintering densification is diffusion of oxygen anions through vacancies,[45] since diffusion coefficient of oxygen anion is several orders of magnitude lower than those of magnesium and aluminum cations.[46-48] Stoichiometry of $MgAl_2O_4$ (expressed by $n$ in $MgO \cdot nAl_2O_3$) often varies during sintering due to MgO vaporization, which occurs preferentially at surfaces and grain boundaries.[8,49-52] Oxygen vacancies ($V_O^{\cdot\cdot}$) are likely to be the principal charge compensating defects, and hence the electrical compensation in Mg-depleted spinel occurs by the anion vacancy defect.[53] The oxygen diffusion in Al-rich spinel is therefore higher than that of the stoichiometric spinel,[54] and densification is enhanced by generation of oxygen anion vacancies associated with the Mg evaporation.[8]

## 2 | EXPERIMENTAL PROCEDURE

### 2.1 | Conventional sintering

The starting material used in this study was $MgAl_2O_4$ spinel powder (S30CR; Baikowski, La-Balme-de-Sillingy, France) with a purity of 99.5% and an initial particle size of 250 nm. The maximum impurities determined by inductively coupled plasma mass spectrometry (ICP) were Ca <9.9 ppm, Fe <2.1 ppm, K <91 ppm, Na <33 ppm, and Si <6.3 ppm. In order to evaluate the sintering behavior, the green compact of $MgAl_2O_4$ (theoretical density of 3.58 g/$cm^3$)[10] with a density of >0.45 was subjected to dilatometry, using a push rod dilatometer (Netzsch 402C, Selb, Germany). Further the green compacts were conventionally sintered by following a schedule of 30°C-500°C at a heating rate of 2°C/min followed by heating to the peak temperature of 1650°C at a heating rate of 3°C/min for a soaking time of 5 hour. Density measurement was carried out by the Archimedes method.

### 2.2 | Flash-sintering experiments

The raw powder was mixed with 5 wt% polyvinyl alcohol in water. The slurry was dried at 90°C in an oven and ground to powder in a zirconia mortar and pestle. The resulting powder was uniaxially pressed at 200 MPa in a dog bone-shaped die, to a green density of 0.45 ± 0.005 of the theoretical density. The dimensions of the gauge portion were 3.3 mm in width, 1.4 mm in thickness, and 20 mm in length. The dog bone-shaped specimen was suspended into the center of a furnace in air by two platinum wires attached to the handles of the dog bone specimen.[39] A constant DC voltage ranged from 300 to 1000 V/cm was applied to the specimen by a high-voltage power supply

(HAR-3P100; Matsusada Precision, Shiga, Japan). The current limit at the power supply was set to 60 mA. The furnace temperature was raised at the heating rate of 10°C/min up to 1410°C in air. The power supply was switched to current control when the current reached the limit value. The voltage supply and furnace were turned off 60 seconds after the flash event. A CCD camera recorded the sample dimensions through a quartz window positioned in front of the furnace. The temperature of the specimen was concurrently measured by a pyrometer (IR-CAS; Chino, Tokyo, Japan) through another quartz window positioned behind the furnace. The densities of the sintered bodies were measured by Archimedes method.

### 2.3 | Microstructure characterization

The microstructure of the sintered bodies was characterized by scanning electron microscopy (SEM, SU-8000; Hitachi, Tokyo, Japan). The average grain sizes of the present specimens were estimated by $\pi/2$ times the average linear intercept length[55] of more than 300 grains in the SEM photographs of the polished and thermally etched surface of the sintered bodies. Thermal etchings for the flash-sintered and conventionally sintered specimens were carried out in air at 1300°C for 30 minute and 1600°C for 30 minute, respectively.

## 3 | RESULTS

Conventional densification behavior obtained from the dilatometric measurement of the green compact heated up to 1650°C is shown in Figure 1A. A SEM image of the specimen sintered at 1650°C for 5 hour is presented in Figure 1B. The final density of the conventionally sintered material was found to be 99.6% of the theoretical density, and average grain size determined from SEM images was 80 μm.

The densification curves for the $MgAl_2O_4$ materials measured for different applied DC field values as a function of the furnace temperature are shown in Figure 2. The data for conventional sintering, without an electric field, are shown as 0 V/cm. The $MgAl_2O_4$ at 0 V/cm (conventional sintering) exhibited a final relative density of 68.6% after the temperature rising up to 1410°C. At the fields from 300 to 750 V/cm, the final densities at the end of the sintering experiments were only slightly increased, and the fields have not exhibited significant effect on the densification behavior of the $MgAl_2O_4$. At 1000 V/cm, FAST[27,28] is followed by flash-sintering, which is characterized by almost vertical slopes of the shrinkage curves; the densification is accelerated at temperatures greater than 1200°C with the final density of 97.9% being achieved at 1410°C.
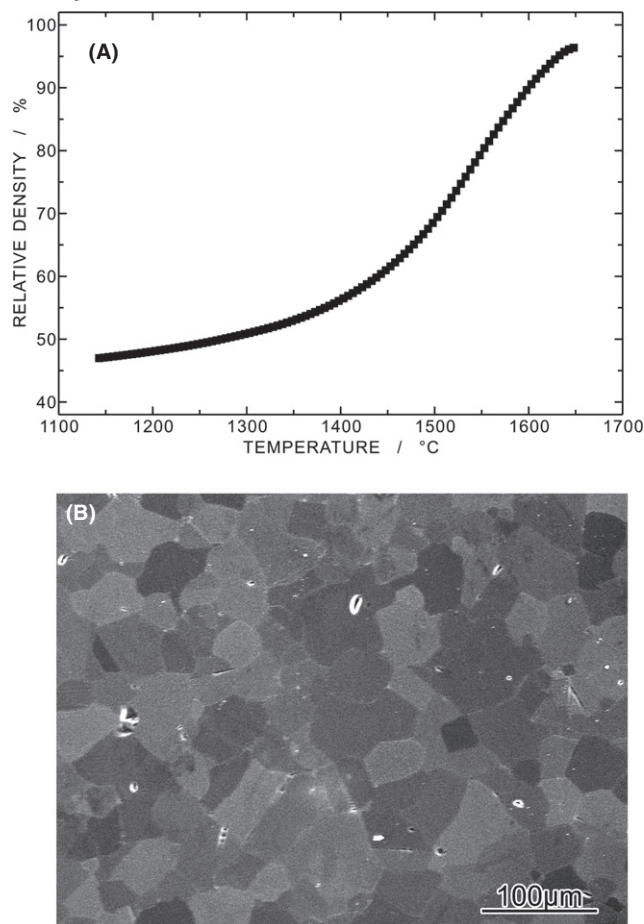
**FIGURE 1** (A) Densification curve in the $MgAl_2O_4$ green compact heated up to 1650°C in air under the conventional sintering condition, and (B) a SEM image of the specimen conventionally sintered at 1650°C for 5 h
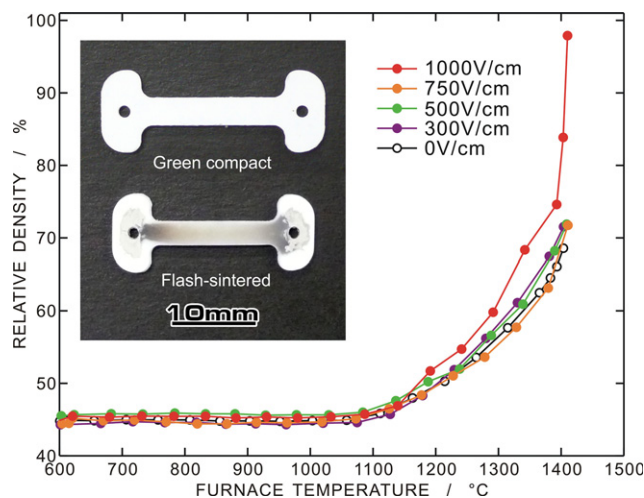
The temperature for the onset of the flash was 1408°C at 1000 V/cm. The flash-sintering can reduce the furnace temperature required for full densification of the spinel. Photographs of the specimens before and after the flash-sintering at 1000 V/cm are inserted in Figure 2. After the occurrence of flash event, the color of the gauge portion became gray, indicating reduction in the specimen during the flash event. The color change was seen only in the flash-sintered specimen. Reduced state associated with flash-sintering has been observed by electron energy loss spectroscopy (EELS) analysis in $Y_2O_3$.[39]

The electric power densities expended during sintering under different fields in the $MgAl_2O_4$ are plotted as a function of inverse of the furnace temperature in Figure 3. At the fields from 300 to 750 V/cm, the logarithm of the power density almost linearly increased with the increasing furnace temperature. At 1000 V/cm, the power dissipation also linearly increased, but deviated from the linearity at about 1400°C; the power density is found to be abruptly increased corresponding to the occurrence of the flash. The nonlinearity occurs at the electric power density of about 20 $mW/mm^3$. According to the previous reports, the onset of the flash event occurs at the power density in a range of 10-50 $mW/mm^3$ in various oxides including electrically conducting, semiconducting and dielectric materials.[29-39] The present material $MgAl_2O_4$ spinel is also found to obey the empirical rule.

Scanning electron microscopy micrographs for the specimens are shown in Figure 4: heated up to 1410°C under (A) 0 V/cm (ie, conventional sintering), (B) 750 V/cm, and (C) 1000 V/cm (flash-sintering regime). The $MgAl_2O_4$ sintered under 0 V/cm exhibits a fine grain size of about



**FIGURE 2** Relative density of the $MgAl_2O_4$ specimens with different DC fields as a function of the furnace temperature. The data for the conventional sintering (0 V/cm) are denoted by the open circles for comparison. Photograph of the specimens before and after the flash-sintering at 1000 V/cm is inserted [Color figure can be viewed at wileyonlinelibrary.com]
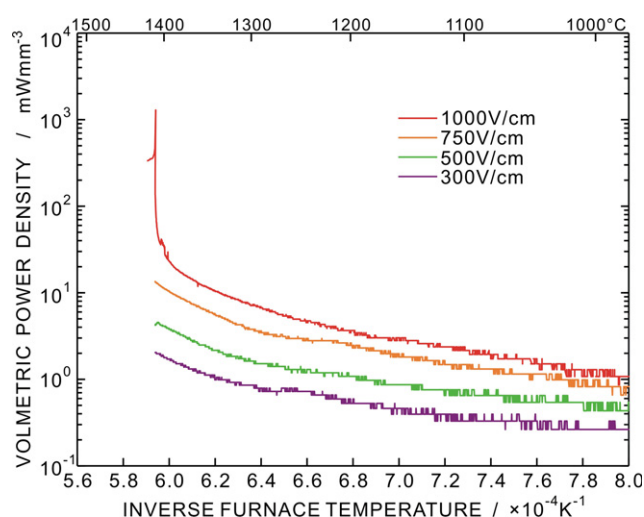


**FIGURE 3** Volumetric power density expended for the sintering experiments at different fields as a function of the inverse of the furnace temperature in the $MgAl_2O_4$ [Color figure can be viewed at wileyonlinelibrary.com]
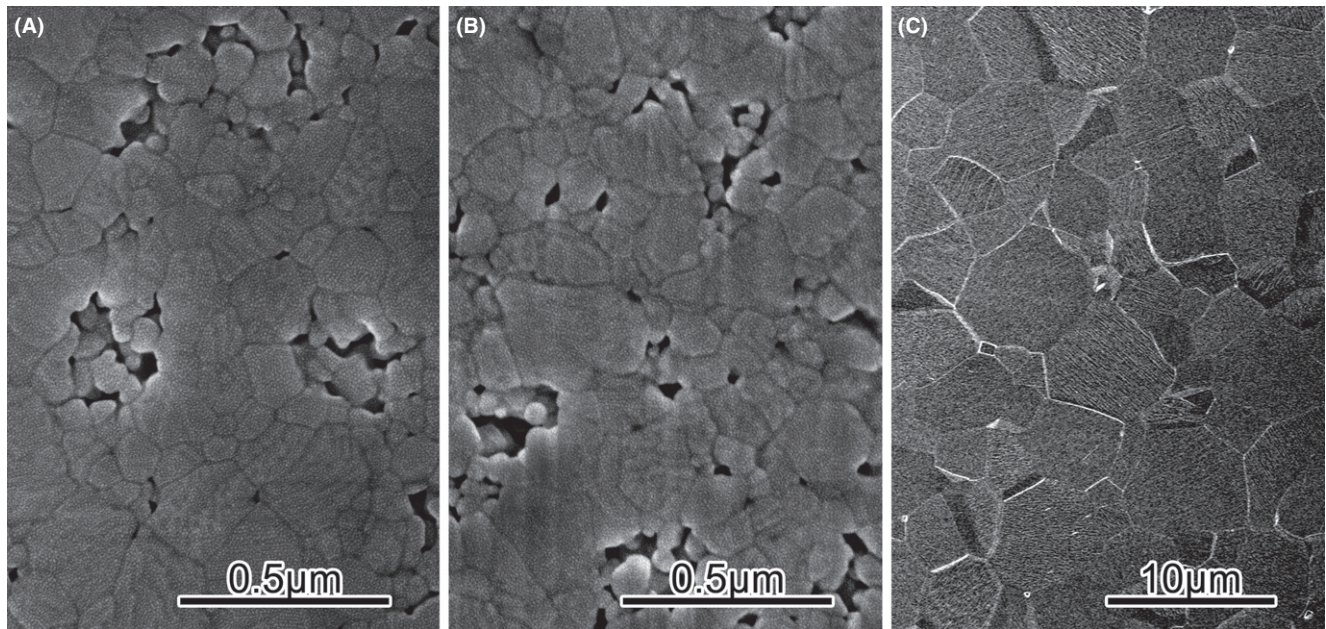
**FIGURE 4** SEM images of the MgAl$_2$O$_4$ bodies sintered under the following conditions: (A) heated up to 1410°C at the field of 0 V/cm (conventional sintering), (B) heated up to 1410°C at 750 V/cm, and (C) flash-sintered at 1000 V/cm

200 nm. The grain size of the specimen sintered to 1410°C at 750 V/cm is marginally larger. However, the grain size of the flash-sintered specimen, (C), is about 5 μm, which is much larger than those of the specimens sintered under lower fields. The flash-sintering process obviously produces rapid grain growth in the MgAl$_2$O$_4$ Specimens. The average grain sizes estimated from the SEM images in the MgAl$_2$O$_4$ bodies are listed in Table 1. The occurrence of the flash definitely enhanced the grain growth rate during densification. It should be noted that the flash-sintered MgAl$_2$O$_4$ exhibited much smaller grain size than the spinel conventionally sintered at 1650°C, though both of the specimens were densified close to the theoretical values indicating that flash-sintering is effective to reduce the grain size of the densified spinel body.

Microstructure gradient along the gauge section was observed in the flash-sintered specimen as follows. Figure 5 shows (A) a schematic of specimen geometry and observed locations, (B) corresponding SEM images at each location, and (C) average grain sizes obtained from the different locations of the flash-sintered specimen. The observation areas A and E were located 2.3 mm apart from the negative and positive electrodes, respectively. The SEM

images indicate that the flash-sintered specimen showed monotonical grain size gradient through the gauge section; the average grain size gradually increases toward the positive electrode. Figure 5C indicates that the average grain size in the flash-sintered sample monotonically increased with the increasing distance from the negative electrode.

The temperatures of the MgAl$_2$O$_4$ specimens measured by a pyrometer under the fields of 300 and 1000 V/cm are plotted as a function of the furnace temperature in Figure 6. The pyrometer temperature and furnace temperature, as expected, well agreed at 300 V/cm. At 1000 V/cm, in contrast, the specimen temperature begins to rise above the furnace temperature beyond 1405°C, and further increasing rapidly to 1667°C, while the furnace temperature is 1410°C. The rapid increase in the specimen temperature results from Joule heating, as previously shown in our study of Y$_2$O$_3$.[36]

The abrupt rise of the power dissipation in Figure 3 was attributed to surge current of the specimen. The electrical conductivity ($\sigma$) during the sintering experiments under the electric fields was calculated by the following equation:

$$\sigma = \frac{I}{V}\frac{L}{A} \quad (1)$$

where $I$ is the current, $V$ is the applied voltage, and $L$ and $A$ are the length and cross-sectional area of the gauge section, respectively.[56] An Arrhenius plot of the electric conductivity as a function of specimen temperature measured by the pyrometer during sintering experiment under 1000 V/cm is shown in Figure 7. For the calculations, the geometry of the gauge section was approximated using the

**TABLE 1** Average grain sizes estimated from SEM images in the MgAl$_2$O$_4$ bodies at different field strength

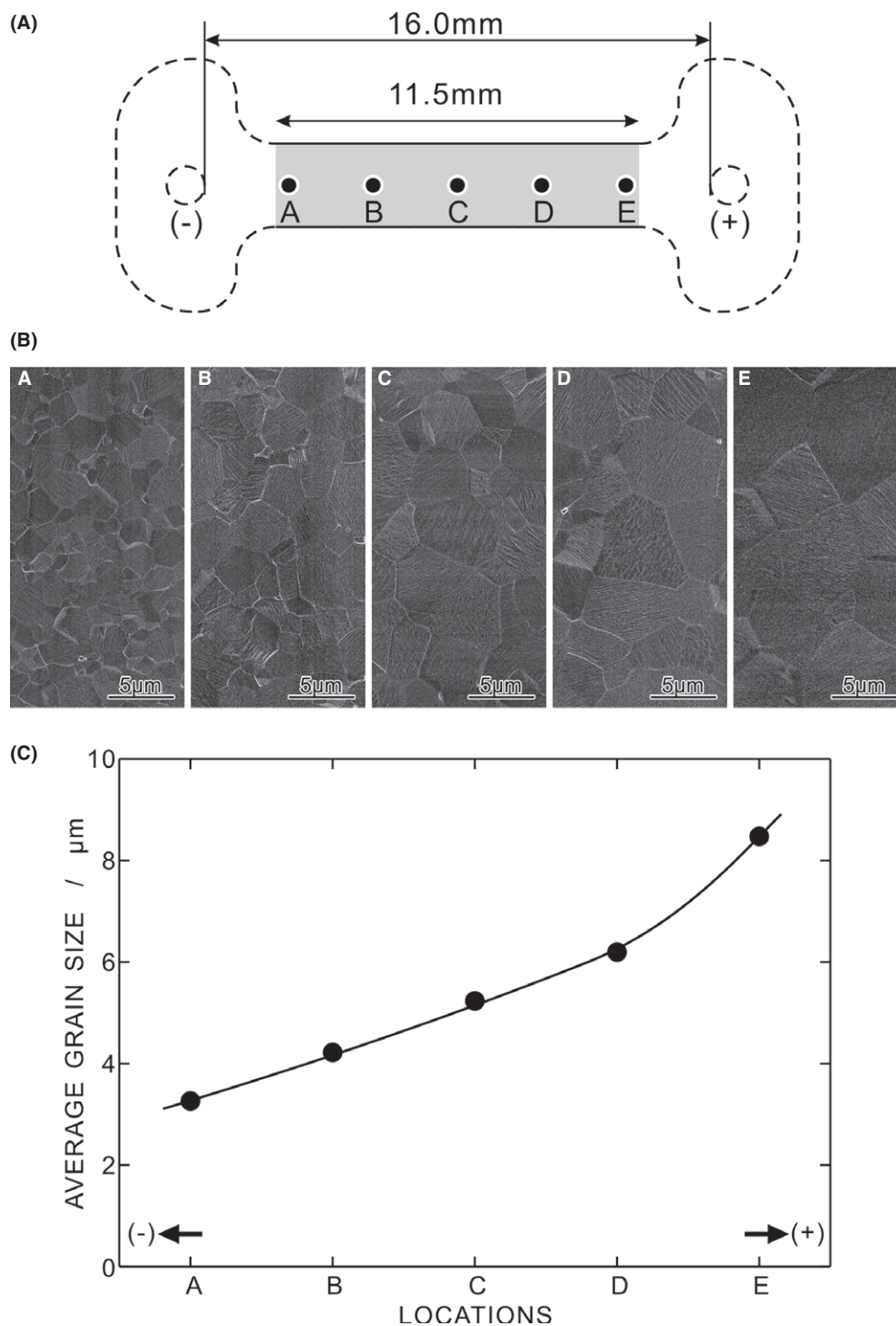| Field strength per V/cm | 0 | 300 | 500 | 750 | 1000 |
|---|---|---|---|---|---|
| Average grain size/μm | 0.199 | 0.200 | 0.200 | 0.203 | 5.23 |

**FIGURE 5**  (A) A schematic of the specimen geometry and observed locations, (B) corresponding SEM images at each location, and (C) average grain sizes obtained from the different locations of the $MgAl_2O_4$ specimen flash-sintered at 1000 V/cm

initial dimensions of the specimen. The conductivity data shows linearity at temperatures lower than 1300°C, but gradually deviates from the linearity in the FAST regime just before the onset of flash event (at 1350°C-1400°C), and then both conductivity and specimen temperature drastically increases after the onset of the flash. The increased specimen temperature and conductivity after the onset of the flash beyond 1410°C must be due to Joule heating. However, the conductivity also increased before the sudden increase in the specimen temperature due to the Joule heating. The increased conductivity observed in the FAST regime must trigger the surge current and Joule heating.
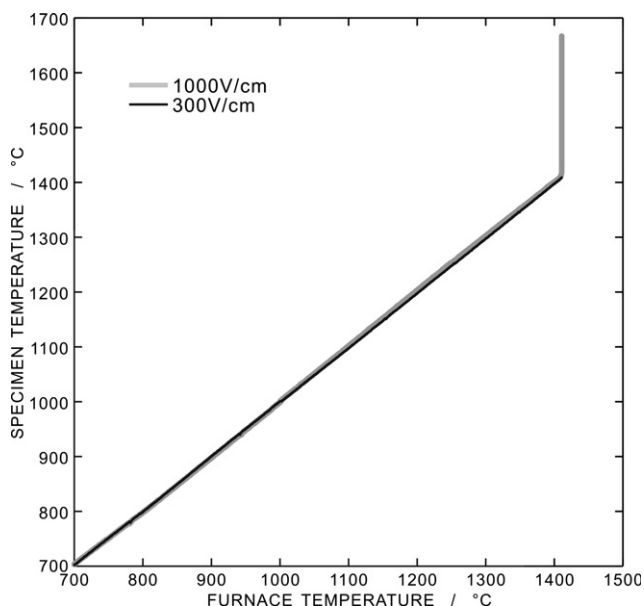
**FIGURE 6** Specimen temperatures measured by a pyrometer under the fields of 300 and 1000 V/cm as a function of the furnace temperature
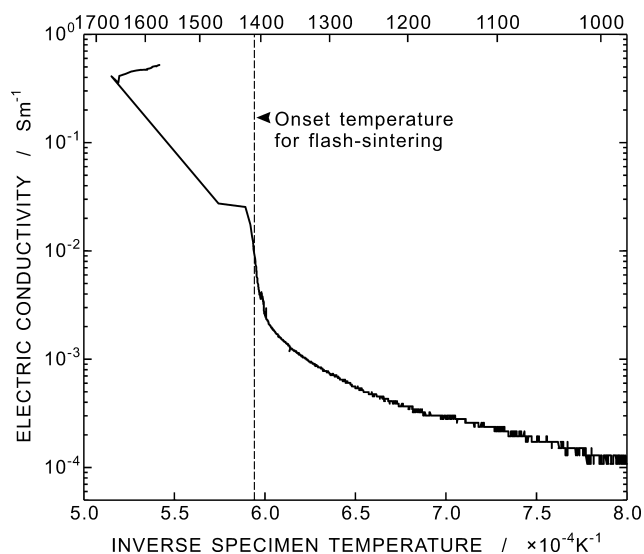


**FIGURE 7** Arrhenius plot of electrical conductivity during the sintering experiments at the field of 1000 V/cm as a function of inverse of specimen temperature measured by the pyrometer

## 4 | DISCUSSION

The present $MgAl_2O_4$ showed flash sintering preceded by FAST at 1000 V/cm. The abrupt increase in the specimen temperature was observed corresponding to the flash event. According to the literature, sudden temperature increase due to Joule heating is mainly responsible for flash-sintering phenomena.[36,57-59] The hybrid behavior in which the flash-sintering is preceded by partial densification by FAST has also been seen in $Al_2O_3$,[31] $TiO_2$[35] and the $Al_2O_3$-

50 vol% tetragonal $ZrO_2$ polycrystal (TZP) composite,[60] but not significantly in the $Y_2O_3$-stabilized $ZrO_2$[27,29] and $Co_2MnO_4$.[30] It has been pointed out that the significant contribution of the flash-sintering is likely to result from an increased conductivity.[31,35,36,39] Since $MgAl_2O_4$ is a dielectric material, the FAST followed by the flash event observed in this study is consistent with the previous results. Sufficient quantity of charge carrier density is probably required for the onset of the flash in the dielectric material. As shown in Figure 7, the electrical conductivity gradually increased just before the sudden temperature increase, and drastically increased during the flash event due to the Joule heating. The rise of the conductivity suggests that charge carrier density increased ahead of the significant Joule heating and the onset of the flash. The presence of incubation stage before the onset of flash has been pointed out in the literature.[60,61]

The grain size distribution shown in Figure 5 could be originated from inhomogeneous temperature distribution in the gauge section. Further detailed measurement of the temperature distribution in the specimen is required during flash event by thermographic analysis. Recent numerical investigations,[62-64] however, have shown that electric field and temperature are homogeneous within the gauge portion during flash event. Holland et al. has reported that no significant temperature difference between grain boundary and grain interior is expected in mixed or ionically conducting ceramic compact;[62] thermal gradients are promptly relaxed by thermal conduction. Qin et al. has shown that grain size is identical within the gauge section of flash-sintered, TZP specimen, and confirmed by FEM analysis that electric field is homogeneous within the gauge section under DC electric field.[64] Therefore, another mechanism that acts in addition to temperature distribution may be responsible for the microstructure gradient through the gauge section in the flash-sintered specimen.

It has been pointed out that densification and grain growth in $MgAl_2O_4$ are accelerated by generation of oxygen anion vacancies owing to the Mg evaporation.[8] In addition, according to the literature, the main charge carrier in $MgAl_2O_4$ is magnesium cation vacancy.[40-44] It would therefore seem that the migration of $Mg^{2+}$ and $V''_{Mg}$ was the dominant conduction mechanism in the FAST regime. $Mg^{2+}$ and $V''_{Mg}$ would migrate to the negative and positive electrodes, respectively, and the electric neutrality in Mg-depleted spinel could be maintained by oxygen anion vacancies at the gauge portion where concentration of $V''_{Mg}$ was high.[53] Gradient of the concentration of $V''_{Mg}$ and $V^{··}_O$ could be thereby produced through the gauge section between the electrodes. When the flash-sintering took place, the diffusional mass transport in the $MgAl_2O_4$ was enhanced by the Joule heating. The grain growth rate could be accelerated especially in the positive side of the gauge

section owing to the relatively high density of oxygen vacancies, as shown in Figure 5C.

It would seem that the rise of the conductivity in the FAST regime could trigger the abrupt increase in temperature due to the Joule heating, leading to the onset of the flash. Diffusional mass transport could be concurrently enhanced by an avalanche of the increased temperature and conductivity due to the Joule heating, resulting in the short time densification in the present material.

# 5 | CONCLUSIONS

In this study, the flash-sintering was employed to consolidate $MgAl_2O_4$ polycrystal from the commercially available raw powder. The fields lower than 750 V/cm had insignificant effect on the sintering behavior, but the spinel can be close to theoretical density by flash-sintering preceded by FAST at 1410°C under the DC field of 1000 V/cm, however, the conventional sintering required higher temperature of 1650°C for full density. The abrupt increase in power dissipation was observed corresponding to the occurrence of the flash event. The grain size in the flash-sintered specimen was significantly larger than those in the specimens sintered under 0-750 V/cm. The mass transport in the spinel was highly enhanced during the flash event. The gradual increment of the specimen conductivity was observed just before the occurrence of flash-sintering; the increased specimen conductivity during the FAST regime led to the progressive Joule heating within the specimen. The increased specimen temperature triggered further increment of current and Joule hearing, and the avalanche of these consequently resulted in the immediate densification.

## REFERENCES

1. Ganesh I. A review on magnesium aluminate ($MgAl_2O_4$) spinel: synthesis, processing and applications. *Int Mater Rev*. 2013;58:63–112.

2. Braulio MAL, Zinngrebe EW, van der Laan SR, Pandolfelli VC. Steel ladle well block post mortem analysis. *Ceram Int*. 2012;38:1447–1462.

3. Rodríguez E, Castillo G-A, Contreras J, et al. Hercynite and magnesium aluminate spinels acting as a ceramic bonding in an electrofused MgO-CaZrO$_3$ refractory brick for the cement industry. *Ceram Int*. 2012;38:6769–6775.

4. Rodríguez EA, Castillo G-A, Das TK, et al. $MgAl_2O_4$ spinel as an effective ceramic bonding in a MgO-CaZrO$_3$ refractory. *J Eur Ceram Soc*. 2013;33:2767–2774.

5. Li J-H, Cai B-Y, Feng W-W, Liu Y-Q, Ma H-W. Investigations on phase constitution, mechanical properties and hydration kinetics of aluminous cements containing magnesium aluminate spinel. *Ceram Int*. 2013;39:8393–8400.

6. Ghosh C, Ghosh A, Haldar MK. Studies on densification, mechanical, micro-structural and structure-properties relationship of magnesium aluminate spinel refractory aggregates prepared from Indian magnesite. *Mater Characterization*. 2015;99:84–91.

7. Gehre P, Aneziris CG, Berek H, Parr C, Reinmöller M. Corrosion of magnesium aluminate spinel-rich refractories by sulphur-containing slag. *J Eur Ceram Soc*. 2015;35:1613–1620.

8. Ting C-J, Lu H-Y. Deterioration in the final-stage sintering of magnesium aluminate spinel. *J Am Ceram Soc*. 2000;83:1592–1598.

9. du Merac MR, Reimanis IE, Kleebe H-J. Electrochemical impedance spectroscopy of transparent polycrystalline magnesium aluminate ($MgAl_2O_4$) spinel. *J Am Ceram Soc*. 2015;98:2130–2138.

10. Chiang Y-M, Kingery WD. Grain-boundary migration in nonstoichiometric solid solutions of magnesium aluminate spinel: I, grain growth studies. *J Am Ceram Soc*. 1989;72:271–277.

11. Ting CJ, Lu HY. Hot-pressing of magnesium aluminate spinel-II. Microstructure development. *Acta Mater*. 1999;47:817–830.

12. Reimanis IE, Kleebe HJ. A review on the sintering and microstructure development of transparent spinel ($MgAl_2O_4$). *J Am Ceram Soc*. 2009;92:1472–1480.

13. Wang CT, Lin LS, Yang SJ. Preparation of $MgAl_2O_4$ spinel powders via freeze-drying of alkoxide precursors. *J Am Ceram Soc*. 1992;75:2240–2243.

14. Bhaduri S, Bhaduri SB. Microstructural and mechanical properties of nanocrystalline spinel and related composites. *Ceram Int*. 2002;28:153–158.

15. Goldstein A, Goldenberg A, Yeshurun Y, Hefetz M. Transparent $MgAl_2O_4$ spinel from a powder prepared by flame spray pyrolysis. *J Am Ceram Soc*. 2008;91:4141–4144.

16. Biswas P, Rajeswari K, Ramavath P, Johnson R, Maiti HS. Fabrication of transparent spinel honeycomb structures by methyl cellulose-based thermal gelation processing. *J Am Ceram Soc*. 2013;96:3042–3045.

17. Frage N, Cohen S, Meir S, Kalabukhov S, Dariel MP. Spark plasma sintering (SPS) of transparent magnesium-aluminate spinel. *J Mater Sci*. 2007;42:3273–3275.

18. Morita K, Kim BN, Hiraga K, Yoshida H. Fabrication of transparent $MgAl_2O_4$ spinel polycrystal by spark plasma sintering processing. *Scr Mater*. 2008;58:1114–1117.

19. Goldstein A, Giefman L, Ziv SB. Susceptor assisted microwave sintering of $MgAl_2O_4$ powder at 2.45 GHz. *J Mater Sci Lett*. 1998;17:977–979.

20. Aliquoat M, Mazo L, Desgardin G, Raveau B. Microwave sintering of spinel-type oxides. *J Am Ceram Soc*. 1990;73:2515–2518.

21. Goldstein A, Kaplan WD, Singurindi A. Liquid assisted sintering of SiC powders by MW (2.45 GHz) heating. *J Eur Ceram Soc*. 2002;22:1891–1896.

22. Munir ZA, Anselmi-Tamburini U. The effect of electric field and pressure on the synthesis and consolidation of materials: a review of the spark plasma sintering method. *J Mater Sci*. 2006;41:763–777.

23. Orrù R, Licheri R, Locci AM, Cincotti A, Cao G. Consolidation/synthesis of materials by electric current activated/assisted sintering. *Mater Sci Eng, R*. 2009;63:127–287.

24. Grasso S, Sakka Y, Maizza G. Electric current activated/assisted sintering (ECAS): a review of patents 1906-2008. *Sci Technol Adv Mater*. 2009;10:053001.

25. Groza JR, Zavaliangos A. Sintering activation by external electrical field. *Mater Sci Eng, A*. 2000;287:171–177.

26. Yang D, Raj R, Conrad H. Enhanced sintering rate of zirconia (3Y-TZP) through the effect of a weak dc electric field on grain growth. *J Am Ceram Soc*. 2010;93:2935–2937.

27. Cologna M, Rashkova B, Raj R. Flash sintering of nanograin zirconia in <5 s at 850°C. *J Am Ceram Soc*. 2010;93:3556–3559.

28. Raj R, Cologna M, Francis JSC. Influence of externally imposed and internally generated electrical fields on grain growth, diffusional creep, sintering and related phenomena in ceramics. *J Am Ceram Soc*. 2011;94:1941–1965.

29. Downs JA, Sglavo VM. Electric field assisted sintering of cubic zirconia at 390°C. *J Am Ceram Soc*. 2011;96:1342–1344.

30. Prette ALG, Cologna M, Sglavo VM, Raj R. Flash-sintering of $Co_2MnO_4$ spinel for solid oxide fuel cell applications. *J Power Sources*. 2011;196:2061–2065.

31. Cologna M, Francis JSC, Raj R. Field assisted and flash sintering of alumina and its relationship to conductivity and MgO-doping. *J Eur Ceram Soc*. 2011;31:2827–2837.

32. Karakuscu A, Cologna M, Yarotski D, et al. Defect structure of flash-sintered strontium titanate. *J Am Ceram Soc*. 2012;95:2531–2536.

33. Zapata-Solvas E, Bonilla S, Wilshaw PR, Todd RI. Preliminary investigation of flash sintering of SiC. *J Eur Ceram Soc*. 2013;33:2811–2816.

34. Schmerbauch C, Gonzalez-Julian J, Röder R, Ronning C, Guillon O. Flash sintering of nanocrystalline zinc oxide and its influence on microstructure and defect formation. *J Am Ceram Soc*. 2014;97:1728–1735.

35. Jha SK, Raj R. The effect of electric field on sintering and electrical conductivity of titania. *J Am Ceram Soc*. 2014;97:527–534.

36. Yoshida H, Sakka Y, Yamamoto T, Lebrun J-M, Raj R. Densification behaviour and microstructural development in undoped yttria prepared by flash-sintering. *J Eur Ceram Soc*. 2014;34:991–1000.

37. M'Peko J-C, Francis JSC, Raj R. Field-assisted sintering of undoped $BaTiO_3$: microstructure evolution and dielectric permittivity. *J Eur Ceram Soc*. 2014;34:3655–3600.

38. Uehashi A, Yoshida H, Tokunaga T, Sasaki K, Yamamoto T. Enhancement of sintering rates in $BaTiO_3$ by controlling of DC electric current. *J Ceram Soc Jpn*. 2015;123:465–468.

39. Yoshida H, Morita K, Kim B-N, Sakka Y, Yamamoto T. Reduction in sintering temperature for flash-sintering of yttria by nickel cation-doping. *Acta Mater*. 2016;106:344–352.

40. Bates JL, Garnier JE. Electrical conductivity of $MgAl_2O_4$ and $Y_3Al_5O_{12}$. *J Am Ceram Soc*. 1981;64:C138–C141.

41. Sonder E. Ionic transference numbers and electrical conduction in $MgAl_2O_4$ spinel. *J Am Ceram Soc*. 1983;66:50–53.

42. Martinelli JR, Sonder E, Weeks RA, Zuhr RA. Mobility of cations in magnesium aluminate spinel. *Phys Rev B*. 1986;33:5698–5701.

43. Mathews T, Jacob KT, Hajra JP. Electrical transport in magnesium aluminate. *Bull Mater Sci*. 1990;13:293–300.

44. Fukatsu N, Kurita N, Shiga H, Murai Y, Ohashi T. Incorporation of hydrogen into magnesium aluminate spinel. *Solid State Ionics*. 2002;152:809–817.

45. Ting C-J, Lu H-Y. Defect reactions and the controlling mechanism in the sintering of magnesium aluminate spinel. *J Am Ceram Soc*. 1999;82:841–848.

46. Bratton RJ. Initial sintering kinetics of $MgAl_2O_4$. *J Am Ceram Soc*. 1969;52:417–419.

47. Bratton RJ. Sintering and grain-growth kinetics of $MgAl_2O_4$. *J Am Ceram Soc*. 1971;54:141–143.

48. Benameur N, Bernard-Granger G, Addad A, Raffy S, Guizard C. Sintering analysis of a fine-grained alumina-magnesia spinel powder. *J Am Ceram Soc*. 2011;94:1388–1396.

49. Sasamoto T, Hara H, Sata T. Mass-spectrometric study of the vaporization of magnesium oxide from magnesium aluminate spinel. *Bull Chem Soc Jpn*. 1981;54:3327–3333.

50. Naghizadeh R, Rezaie HR, Golestani-Fard F. Effect of $TiO_2$ on phase evolution and microstructure of $MgAl_2O_4$ spinel in different atmospheres. *Ceram Int*. 2011;37:349–354.

51. Chiang Y-M, Kingery WD. Grain-boundary migration in nonstoichiometric solid solutions of magnesium aluminate spinel: II, effects of grain-boundary nonstoichiometry. *J Am Ceram Soc*. 1990;73:1153–1158.

52. Nuns N, Béclin F, Crampon J. Grain-boundary characterization in a nonstoichiometric fine-grained magnesium aluminate spinel: effects of defect segregation at the space-charge layers. *J Am Ceram Soc*. 2009;92:870–875.

53. Okuyama Y, Kurita N, Fukatsu N. Defect structure of alumina-rich nonstoichiometric magnesium aluminate spinel. *Solid State Ionics*. 2006;177:59–64.

54. Reddy KPR, Cooper AR. Oxygen diffusion in mafnesium aluminate spinel. *J Am Ceram Soc*. 1981;64:368–371.

55. Fullman RL. Measurement of particle sizes in opaque bodies. *Trans AIME*. 1953;197:447–452.

56. Halliday D, Resnick R, Walker J, *Fundamentals of Physics Extended 8th Edition*. New Jersey: John Wiley & Sons, Inc.; 2008:688–690.

57. Grasso S, Sakka Y, Rendtorff N, et al. Modeling of the temperature distribution of flash sintered zirvonia. *J Ceram Soc Jpn*. 2011;119:144–146.

58. Raj R. Joule heating during flash-sintering. *J Eur Ceram Soc*. 2012;32:2293–2301.

59. Du Y, Stevenson AJ, Vernat D, Diaz M, Marinha D. Estimating Joule heating and ionic conductivity during flash sintering of 8YSZ. *J Eur Ceram Soc*. 2016;36:749–759.

60. Naik KS, Sglavo VM, Raj R. Field assisted sintering of ceramic constituted by alumina and yttria stabilized zirconia. *J Eur Ceram Soc*. 2014;34:2435–2442.

61. Francis JSC, Raj R. Influence of the field and the current limit on flash sintering at isothermal furnace temperatures. *J Am Ceram Soc*. 2013;96:2754–2758.

62. Holland TB, Anselmi-Tamburini U, Quach DV, Tran TB, Mukherjee AK. Effects of local Joule heating during the field

assisted sintering of ionic ceramics. *J Eur Ceram Soc*. 2012;32:3667–3674.

63. Pereira da Silva JG, Lebrun J-M, Al-Qureshi HA, Janssen R, Raj R. Temperature distributions during flash sintering of 8% yttria-stabilized zirconia. *J Am Ceram Soc*. 2015;98:3525–3528.

64. Qin W, Majidi H, Yun J, van Benthem K. Electrode effects on microstructure formation during FLASH sintering of yttrium-stabilized zirconia. *J Am Ceram Soc*. 2016;99:2253–2259.